Sixth International Symposium on Marine Propulsors
smp'19, Rome, Italy, May 2019

Mutual Interference of Propeller Bearing Force Caused by Propeller Distribution

Shuai Sun[1], Yimin Gao[2], Chunyu Guo[1], Chao Wang[1], Yuan Zhang[1]

[1]Department of Naval Architecture and Ocean Engineering, Harbin Engineering University (HEU), Harbin, China
[2]China Ship Development and Design Center (CSDDC), Shanghai, China

ABSTRACT

With improvements in ship design and increasing market demands, the speed and displacement of ships are increasing gradually. Consequently, multiple-propeller ships such as two- and four-propeller ships have been developed in recent years. The propeller performance of such ships is quite different from that of general single-propeller ships owing to the mutual interference of propellers. The computational fluid dynamics method is used to simulate the influence of these two propeller distributions on the propeller performance. First, the hydrodynamic performance and bearing force for a single propeller are calculated. Then, the influence of the lateral distance between two propellers on the propeller bearing force is studied. Finally, an optimal propeller distribution is obtained by integrating the propeller propulsion performance and bearing force performance. This should provide theoretical guidance for the engineering practice of multiple-propeller ships.

Keywords

Propeller distribution, bearing force, fast Fourier transform (FFT), frequency characteristics.

1 INTRODUCTION

A periodical bearing force acts on the stern when a propeller works in a nonuniform flow field in three directions. This force is transferred to the hull through the shaft system and flow, where it acts to increase underwater noise and vibration on the hull. Propeller bearing force was identified by researchers in the early 1960s, but few studies have investigated it since the 1970s. Merz et al. (2005) used a finite element method to analyze the hull structure response and acoustic response under the action of a propeller's axial fluctuating force. Their results indicate that the dynamic response of the shaft system led by the propeller bearing force causes propeller vibration that in turn makes the propeller generate more noise. Kornev et al. (2011) used the unsteady Reynolds-averaged Navier-Stokes–large eddy simulation mixed method to conduct a detailed study of the stern wake flow of KVLCC2. Their results show that the pulsation of propeller thrust in an unsteady wake field is two times that in a time-averaged wake field. Further, the instability of the wake field is very large, and therefore, it must be considered when calculating the unsteady propeller load. Felli et al. (2011) analyzed the energy transfer process in the wake field using power spectral density analysis of the kinetic energy and revealed the propeller wake instability mechanism. Yingsan et al. (2013) used computational fluid dynamics (CFD) to study the unsteady hydrodynamic bearing force of a five-blade propeller of a model submarine, and then, they used a finite element and boundary element model to calculate the hull structure and acoustic response in the frequency domain under the excitation of propeller bearing force. Their calculation results show that the propeller axial force contributes most to the underwater noise of the submarine. Further, the propeller's transverse bearing force is larger than its vertical bearing force, and the fluctuating force of a single blade has a large phase difference with that of the whole propeller. Ye et al. (2013) used theoretical and experimental method to calculate the bearing force of conventional and unconventional propellers and found that the quasi-steady state method can be widely used for calculating the bearing force of conventional propellers whereas it is more reasonable to use theoretical methods including the panel method and lifting surface method for unconventional propellers such as a highly skewed propeller. Chen et al. (2014) used the CFX sliding grid technique to predict the unsteady hydrodynamic performance of a propeller in an axial wake field; their calculation results agreed well with previously reported values. They also analyzed the varying pattern of the propeller bearing force and provided an analysis method for numerically calculating this force.

* The research was financially supported by the National Natural Science Foundation of China (Grant no. 51679052) and by the Defense Industrial Technology Development Program (Grant no. JCKY2016604B001).

The abovementioned studies focused on the propeller bearing force of a single propeller. However, ships often have two and four propellers nowadays, and the influence of these propeller distributions on the propeller bearing force has attracted little research attention. This study focuses on the E779A propeller and calculates its unsteady hydrodynamic performance in different distributions. First, the open water performance of an E779A single propeller is calculated, and the obtained results are compared with test values. Then, the influence of lateral distance on the propeller bearing force is calculated. Time-domain data of the propeller bearing force under different working conditions are monitored, and then, a spectrum curve is obtained through fast Fourier transform (FFT). Finally, the influence of lateral distance on the propeller bearing force under different distributions is summarized.

2 THEORY

The RANS equations for an incompressible flow are written as follows.

$$\frac{\partial u_i}{\partial x_i} = 0 \tag{1}$$

$$\frac{\partial (u_i)}{\partial t} + \frac{\partial}{\partial x_j}\left(u_i u_j\right) = -\frac{\partial p}{\partial x_i} + \frac{\partial \tau_{ij}}{\partial x_j} + S_i \tag{2}$$

In our calculations, we used the $k-\omega$ shear stress transport (SST) turbulence model that is frequently used for calculating the propeller hydrodynamic performance. This model can well simulate complex flows in the presence of flow separation and strong adverse pressure gradients. $Y+$, defined in Eq. (3) below, is the dimensionless distance between the first layer of grid nodes and the wall. There are certain limits on its value (Gaggero et al. 2014); $Y+ = 60$ is generally considered an appropriate value.

$$Y+ = \frac{Y}{\mu}\sqrt{\rho \tau_\omega} \tag{3}$$

where Y is the distance between the unit center and the wall; μ, the kinetic viscosity of a fluid; ρ, the fluid density; and τ_ω, the wall shear stress.

3 CALCULATION MODEL

3.1 Geometric parameters of propeller

We use the E779A propeller as our calculation model (Pereira et al., 2004). Table 1 shows its main geometric parameters and Fig. 1 shows its geometry model.

Table 1 Main geometric parameters of E779A propeller

Geometric parameter	Value
Diameter (mm)	227
Hub ratio	0.2
No. of blades	4
Area ratio (A_e/A_0)	0.689
Rake	4°35’

A large calculation domain, shown in Fig. 2, is required to simulate the propeller’s open water performance. The front inlet and outlet are at 4D and 6D distance from the propeller center, respectively. The section area of the front inlet is 4D × 4D. Here, D is the propeller diameter. To study the influence of propeller distribution on the bearing force, the right side of the calculation domain is set as symmetry; the distribution and calculation domain are respectively shown in Fig. 3(a) and (b), where A is the transverse distance.

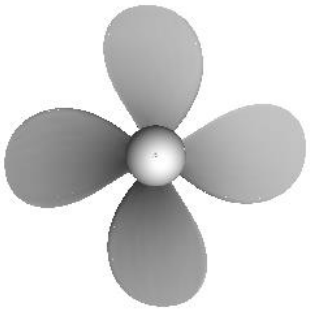

Figure 1 Geometry model

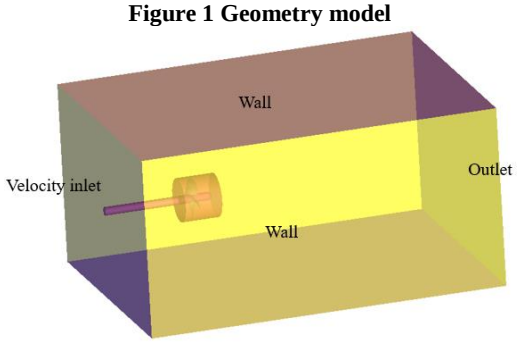

Figure 2 Calculation domain of single propeller

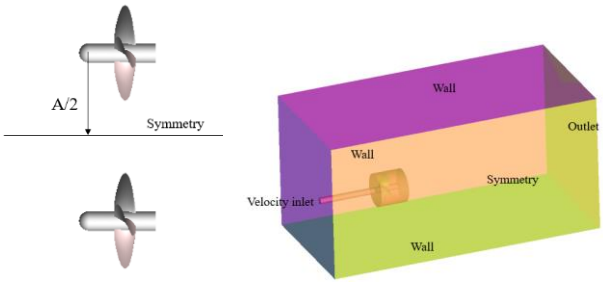

(a) Propeller distribution (b) Calculation domain

Figure 3 Calculation model for two propellers

3.2 Establishing computational domain and setting computational parameters

The steady multiple reference frame (MRF) method was applied and a sliding mesh was used in the unsteady simulation. The internal domain wrapping propeller rotates at 1200 revolutions per minute around the X-axis. The external domain is absolutely static.

The SIMPLEC method is used in this study. For spatial discretization, the pressure is standard and the momentum is second-order upwind. The propeller blades, hub, and outside wall of the far field are all defined as nonslip walls. The inlet is set as a velocity inlet and the outlet is set as a pressure outlet. The gauge pressure is set as 0. The two domains are linked through interfaces. The flow field information is transferred through interface interpolation.

3.3 Grid division

The whole calculation domain is divided into structured grids to improve the computational efficiency. Fig. 4(a) shows the propeller mesh; the thickness of the first layer of grids is 0.2 mm, corresponding to Y+ = ~60. Fig. 4(b) shows the calculation domain grids; the grids of the inner field around the propeller are appropriately refined whereas the far field grids are relatively sparse.

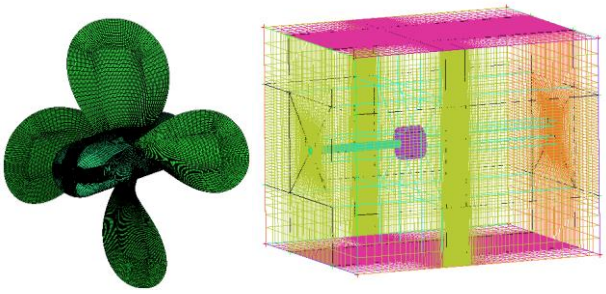

(a) Grids of propeller (b) Grids of external domain

Figure 4 Calculation grids

4 CALCULATION RESULT ANALYSIS

4.1 Validation of calculation method

Three grids were used for grid sensitivity analysis. Table 2 lists the number of cells and calculation results for the design point. When the total number of grids is 3.15M, the CFD results agree well with the experimental fluid dynamics (EFD) results. The error is less than 3%. When the number of grids is increased further, the calculation results hardly change. From the viewpoint of calculation efficiency, Case 2 is applied in the subsequent simulation.

Table 2 Number of grids and calculation results

Description	No. of cells			Thrust	Moment
	Inner field	Far field	Whole	T /N	M /N.m
Case 1	1.22M	1.01M	2.23M	301.25	13.05
Case 2	1.74M	1.41M	3.15M	311.55	13.48
Case 3	2.43M	2.02M	4.45M	312.65	13.56
EFD	———			320.37	13.65
Error 1				5.97%	4.40%
Error 2				2.75%	1.25%
Error 3				2.41%	0.66%

4.2 Results and discussions

Fig. 5 shows the open water hydrodynamic performance. The thrust and torque coefficients are calculated using Eq. (4).

$$K_T = \frac{T}{\rho n^2 D^4}$$
$$K_Q = \frac{Q}{\rho n^2 D^5} \quad (4)$$

Here, T is the propeller thrust; Q, the propeller torque; ρ, the density of water (=998.2 kg/m^3); n, the propeller velocity; and D, the propeller diameter. Fig. 6 shows the contrasting calculation and test results of the pressure coefficient distribution of the section at 0.7R. The pressure coefficient is defined as follows:

$$C_P = (P - P_0) / (1/2 \rho V_R^2) \quad (5)$$

where $(P - P_0)$ is the relative pressure and $V_R = \sqrt{V_x^2 + (2\pi nr)^2}$, the relative inflow velocity. Here, V_x is the axial velocity component and n, the speed of rotation. Fig. 6 shows that the calculation results of the pressure coefficient distribution agree well with the test results reported by Jessup (1982). In particular, in the central area of the blade, the two results are almost consistent. This indicates that the numerical calculation method can accurately simulate the pressure distribution of the blade surface, and the number of grids is also reasonable.

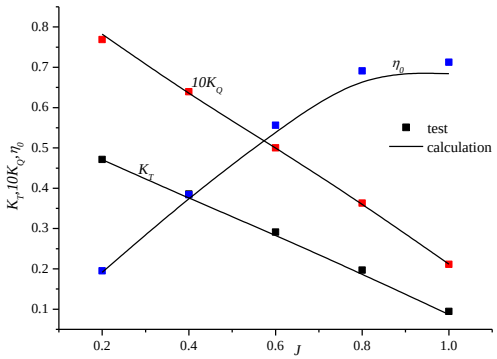

Figure 5 Open water hydrodynamic performance of propeller

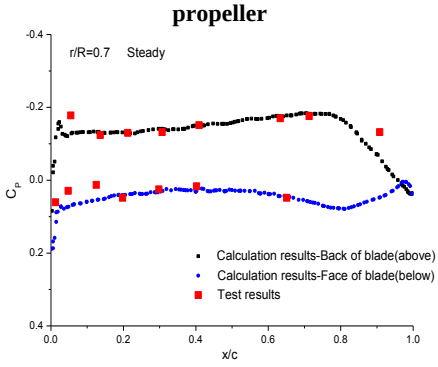

Figure 6 Pressure coefficient distribution of section at 0.7R

After the calculation convergence is stability, time-domain data of six pulsating components of the unsteady propeller bearing force are monitored: thrust, transverse force, vertical force, torque, transverse bending moment, and vertical bending monument. All forces and moments are made dimensionless according to Eq (4), and then, the time-domain curve is transformed into a frequency-domain curve using fast Fourier transform (FFT). Fig. 7 shows the pulsating time-domain curve and frequency-domain curve of the propeller bearing force.

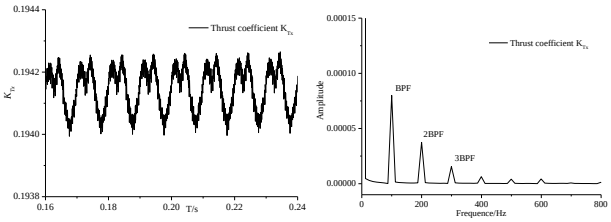

(a) Time-domain data of K_{Tx} (b) Frequency-domain data of K_{Tx}

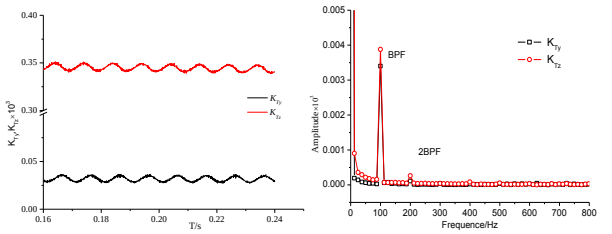

(c) Time-domain data of K_{Ty}, K_{Tz} (d) Frequency-domain data of K_{Ty}, K_{Tz}

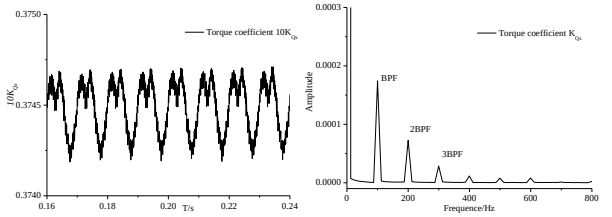

(e) Time-domain data of K_{Qx} (f) Frequency-domain data of K_{Qx}

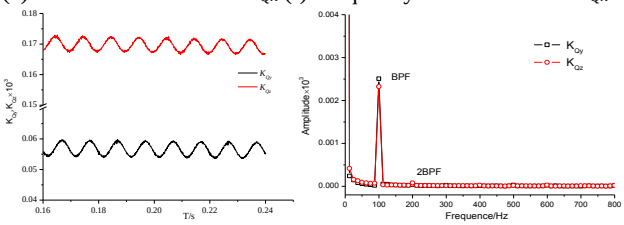

(g) Time-domain data of K_{Qy}, K_{Qz} (h) Frequency-domain data of K_{Qy}, K_{Qz}

Figure 7 Unsteady bearing force of propeller

We used the same method to obtain results with different propeller distributions. Owing to space restrictions, the time-domain curve and frequency-domain curve of the propeller bearing force are omitted. To compare the bearing force for different lateral distances more clearly, the change regulation of the propeller bearing force pulsating peak value (BPF) are shown in Fig. 8. The figure shows that the six pulsating components of the unsteady propeller bearing force have the same regulation. The BPF value dramatically decreases with an increase in the lateral distance between two propellers; when the lateral distance reaches up to 2D (where D is the diameter of the propeller), the BPF value remains roughly constant. It indicates that the lateral distance plays a crucial role in the propeller bearing force and that the distance should be two times larger than the propeller diameter.

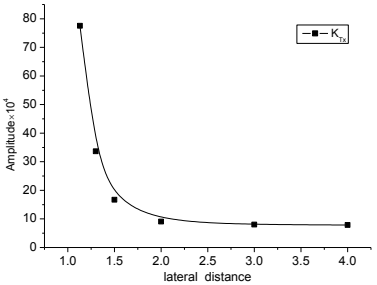

(a) Influence of lateral distance on K_{Tx}

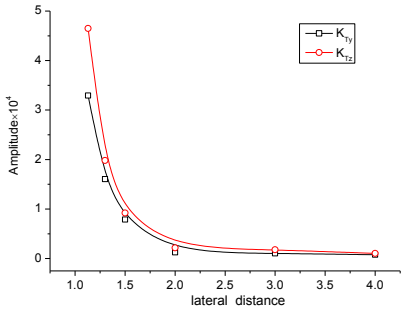

(b) Influence of lateral distance on K_{Ty}, K_{Tz}

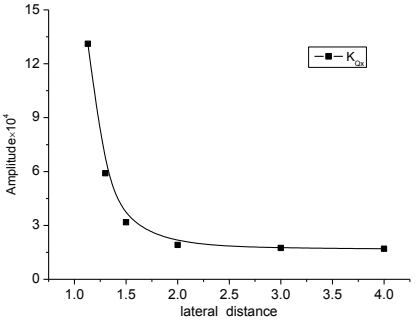

(c) Influence of lateral distance on K_{Qx}

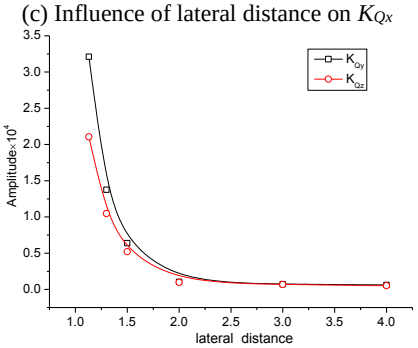

(d) Influence of lateral distance on K_{Qy}, K_{Qz}

Figure 8 Change in propeller bearing force pulsating peak

5 CONCLUSIONS

In this study, the sliding grid technique was used. By adjusting the lateral distance between two propellers, the hydrodynamic performance of the propeller and the induced bearing force were simulated. The calculation results were analyzed, and the following conclusions were derived:

(1) The six pulsating components of the unsteady propeller bearing force vary periodically over time and have the same fluctuation frequency. All show different peak levels that are integral multiples of the BPF, with the peak being the largest at the BPF and attenuating gradually afterwards.

(2) The time-averaged propeller side force and bending moment are smaller than the time-averaged thrust and torque. However, the side force fluctuation is equivalent to the thrust fluctuation, and the bending moment fluctuation is much larger than the torque fluctuation.

(3) The lateral distance plays a crucial role in the propeller bearing force, and the distance between two propellers should be two times larger than the propeller diameter.

This study does not consider cavitation although it can impact the level of bearing force. Therefore, we will investigate cavitation in a future study.

REFERENCES

S.Merz, R. Kinns, N. J. Kessissoglou (2005) Structure and acoustic responses of a submarine hull due to propeller force. J Sound Vib 325:266–286.

Kornev, N., Taranov, A., Shchukin, E., Kleinsorge, L. (2011) Development of hybrid urans–les methods for flow simulation in the ship stern area. J Ocean Eng 38:1831–1838.

Yingsan Wei, Yongsheng Wang (2013) Unsteady hydrodynamics of blade forces and acoustic responses of a model scaled submarine excited by propeller's thrust and side-forces. J of Sound Vib 332: 2038-2056.

Ye Jingming, Xiong Ying, Pen Youwen (2013) Analysis of prediction method of forces exerted on propeller bearing. J Ship Eng 03: 16-18.

Tan Yanshou, He Wei (2006) Calculation of unsteady shaft forces of propeller (in Chinese). J Ship Ocean Eng 02:42-46.

Chen Ruxing, Zhou Ruiping, Lin Xichen (2014) Numerical simulation of the propeller-induced force based on CFX (in Chinese). J Wuhan Univ Technol 07: 73-79.

Feng Xuemei, Lu Chuanjing, Wu Qiong, Cai Rongquan (2012) Numerical Simulation of Propeller Cavitation in Uniform Flow (in Chinese). J Shipbuilding of China 03: 18-27.

Hu Jian (2006) Research on propeller cavitation characteristics and low noise propeller design. D Harbin Eng Univ.

ITTC Propulsion Committee (1998). In: Proceedings of propeller RANS/Panel method workshop, Grenoble, France.

Jessup, S (1982) Measurements of the pressure distribution on two model propellers. J Technical report, DTNSRDC82/035.

S.Gaggero, D.Villa, S.Brizzolara (2010) RANS and PANEL method for unsteady flow propeller analysis. In: Proceedings of the 9th International Conference on Hydrodynamics.

Krasilnikov V, Zhang Z, Hong F (2009) Analysis of unsteady propeller blade forces by RANS. In: First international symposium on marine propulsors smp'09, Trondheim, Norway.

Leishmann JG, Beddoes TS (1989) A semi-empirical model for dynamic stall. J Am Helicopter Soc 34(3):3–17.

Qiu Zhenliang (1999) Investigation on the transverse force of propeller oblique flow effect upon the maneuver of river boat (in Chinese). J Nav China 02: 38-42.

Blake, W.K (1996) Mechanics of flow-induced sound and vibration. Orlando Academic Press Inc.

Li Liang, Wang Chao, Sun Shengxia, Sun Shuai (2015) Numerical prediction analysis of propeller bearing force for hull-propeller-rudder system (in Chinese). J Wuhan Univ Technol 39: 768-772.